Correlation-Enhanced Interaction of a Bose-Einstein Condensate with Parametric Magnon Pairs and Virtual Magnons

Victor S. L'vov,[1,2,*] Anna Pomyalov,[2,†] Dmytro A. Bozhko,[3,‡] Burkard Hillebrands,[4,§] and Alexander A. Serga[4,‖]
[1]*Department of Complex Systems, Weizmann Institute of Science, Rehovot 76100, Israel*
[2]*Department of Chemical and Biological Physics, Weizmann Institute of Science, Rehovot 76100, Israel*
[3]*Department of Physics and Energy Science, University of Colorado Colorado Springs, Colorado Springs, Colorado 80918, USA*
[4]*Fachbereich Physik and Landesforschungszentrum OPTIMAS, Rheinland-Pfälzische Technische Universität Kaiserslautern-Landau, 67663 Kaiserslautern, Germany*

(Received 16 May 2023; revised 13 July 2023; accepted 7 September 2023; published 13 October 2023)

Nonlinear interactions are crucial in science and engineering. Here, we investigate wave interactions in a highly nonlinear magnetic system driven by parametric pumping leading to Bose-Einstein condensation of spin-wave quanta—magnons. Using Brillouin light scattering spectroscopy in yttrium-iron garnet films, we found and identified a set of nonlinear processes resulting in off-resonant spin-wave excitations—virtual magnons. In particular, we discovered a dynamically strong, correlation-enhanced four-wave interaction process of the magnon condensate with pairs of parametric magnons having opposite wave vectors and fully correlated phases.

DOI: 10.1103/PhysRevLett.131.156705

Nonlinear wave interactions govern the behavior of various systems in nature, including processes in the Earth's ocean and atmosphere [1], in stars [2], and even the evolution of the Universe [3]. In the field of magnetism, the use of nonlinear phenomena opens promising prospects for applications of magnonics and spintronics in neuromorphic computing, microwave data processing, and nanoscale wave logic circuits [4–11]. Spin waves, or magnons, in magnetically ordered materials are highly nonlinear compared with, for example, phonons or photons in solids. One of the best systems for studies of nonlinear spin-wave phenomena is the single-crystal ferrimagnetic yttrium iron garnet (YIG, $Y_3Fe_5O_{12}$) material [9,12,13]. A strong magnon nonlinearity, combined with a high quality factor of magnons in YIG, facilitates the creation, registration, and study of various interaction processes.

The phenomenon of Bose-Einstein condensation of magnons at the bottom of their frequency spectrum, observed in YIG films [14–20], also develops through the nonlinear scattering of magnons [21]. In our experiments, this condensation was achieved by the parametric pumping [22] of magnons with microwave radiation [14,15,20,21,23–25].

Here, we reveal several nonlinear processes that involve not only "real" quasiparticles—the eigenmodes of the medium—but produce, as a final result, virtual quasiparticles—out-of-resonance waves—caused by various types of nonlinear interactions. The most nontrivial process involves a pair of parametrically excited magnons and a Bose-Einstein condensate (BEC). This process is enhanced by full-phase correlations in parametric magnon pairs with opposite wave vectors $\boldsymbol{q}$ and $-\boldsymbol{q}$.

Previously, virtual quasiparticles (e.g., virtual magnons) appeared in the theory of nonlinear waves [26–29] only as mathematical abstractions, mediating interactions between "real" quasiparticles. At the same time, the experimental observation of virtual quasiparticles is crucial for the identification of possible physical processes in nonlinear wave systems. This is especially critical when, for various reasons, the experimental methods do not allow one to observe the real quasiparticles involved in these processes.

In our studies, we used Brillouin light scattering (BLS) spectroscopy [30,31] employing a triple-pass tandem Fabry-Pérot interferometer [32]. Its high sensitivity enables the detection of a tiny number of magnons even at thermal noise level, and the frequency resolution (as low as 50 MHz) is quite sufficient for experiments with magnons in the 3–15 GHz range, which was explored in our investigation. The 532 nm laser beam is focused into a 20 μm diameter probing spot in the parametrically pumped area of the YIG film. By setting the incidence angle $\Theta_{q\|}$ of this beam [33], the wave vectors of magnons propagating in the YIG film plane along the line of its intersection with the beam incidence plane are selected. Since, in our case, the incident plane is oriented along the direction of the bias magnetic field $\boldsymbol{H}$, magnons propagating in the same direction with wave vectors $\boldsymbol{q}_{\|} \| \boldsymbol{H}$ are detected. The change

in the incidence angle from 0 to the maximal value of 58° in our experiment corresponds to the change in the detectable wave vectors from 0 to 2×10^5 cm^{-1}. The wave vector resolution in our experiments is of the order of $\pm 10^3$ cm^{-1} [34].

Microwave pumping at 13.2 GHz is applied to the in-plane magnetized 6.7 μm-thick YIG film using a microstrip resonator of 50 μm width. In order to achieve high magnon densities $n(\omega, \boldsymbol{q})$, the pumping is supplied in pulses of up to 20 W and duration of 1 μs. A sufficiently low repetition rate of 1 kHz maintains a thermal quasiequilibrium from pulse to pulse.

Our experimental results for the BLS intensity spectra $I(\omega, q_\parallel)$, proportional to $n(\omega, q_\parallel)$, are shown in Fig. 1. The solid red line shows the calculated magnon frequency spectrum $\omega_{q_\parallel}$ which has two minima $\omega_{\rm bot} \equiv \min_{q_\parallel}\{\omega_{q_\parallel}\} \approx 4 \times (2\pi)$ GHz at $q_\parallel = \pm q_{\rm bot}$ with $q_{\rm bot} \approx 4 \times 10^4$ cm^{-1}. The two brightest spots in the vicinity of the bottom of the magnon spectra at $\pm q_{\rm bot}$ originate from "bottom" magnons associated with the left and right BEC states.

Above these brightest spots we see three spots with $\omega \approx 2\omega_{\rm bot}$ and $q_{\rm left} \approx -2q_{\rm bot}$, $q_{\rm center} \approx 0$, and $q_{\rm right} \approx 2q_{\rm bot}$. It is natural to relate them to the confluence of two bottom magnons [38,39], as shown by green arrows in Fig. 1(a): (i) left spot, $\omega_{-q_\parallel} + \omega_{-q_\parallel} \Rightarrow 2\omega_{\rm bot}$ and $q = -2q_{\rm bot}$; (ii) central spot, $\omega_{-q_\parallel} + \omega_{+q_\parallel} \Rightarrow 2\omega_{\rm bot}$ and $q = 0$; and (iii) right spot, $\omega_{+q_\parallel} + \omega_{+q_\parallel} \Rightarrow 2\omega_{\rm bot}$ and $q = 2q_{\rm bot}$. However, in our magnetization geometry, neither $\omega = 2\omega_{\rm bot}$ with $q = \pm 2q_{\rm bot}$ nor $\omega = 2\omega_{\rm bot}$ with $q = 0$ are eigenmodes of the YIG film chosen. The only plausible explanation [40] builds on the fact that we observe off-resonant waves driven by appropriate nonlinearity, i.e., virtual magnons. For brevity, we will call them "virtual double-bottom" magnons [41].

In Fig. 1(a) the BLS spectra $I(\omega, q_\parallel)$ are supplemented by two down-pointing orange arrows showing the process of parametric pumping by an external quasihomogeneous microwave field with wave vector $\boldsymbol{q}_{\rm pump} \approx 0$ and frequency $\omega_{\rm pump}$. Precisely at this position, we see a rather bright spot, indicating the presence of precession with this wave vector and frequency. Since there is no corresponding magnon eigenmode with $\omega = \omega_{\rm pump}$, we observe here one more type of virtual magnon, called, for concreteness, "virtual pump" magnons. They are directly driven by the external microwave signal through the transverse component of the oscillating magnetic field [23,42,43]. The driving mechanism is similar to the excitation of ferromagnetic resonance (FMR), with the difference that in our experiment the frequency of the excitation force exceeds the FMR frequency by more than 6 GHz, while the FMR linewidth is about 1.5 MHz.

At the same time, we see no BLS response at the frequency of the parametrically pumped real magnons $\omega_{\rm par} = \omega_{\rm pump}/2$ because the wave numbers of the parametric magnons are quite large and lie outside the sensitivity limit

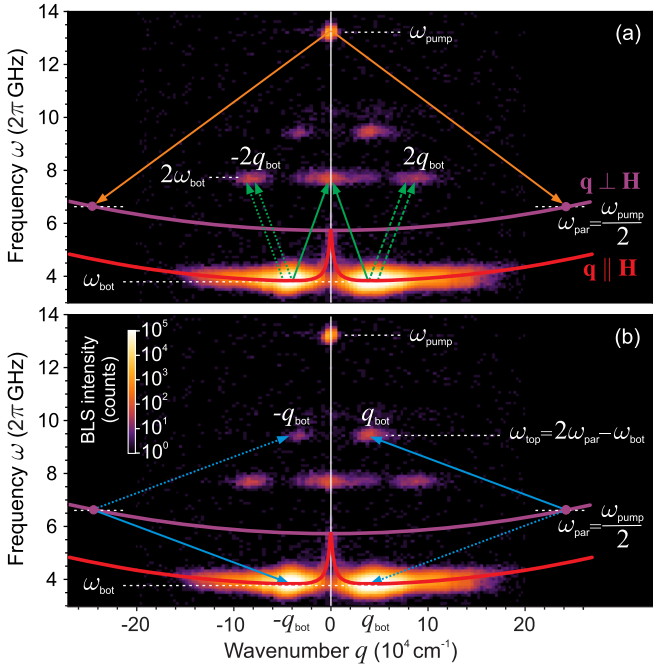

FIG. 1. Frequency- and wave-vector-resolved BLS intensity spectra of real and virtual magnons. The spectra were measured during the action of microwave pumping in a YIG film magnetized in plane by the field $H = 1350$ Oe. The experimental intensity spectra are shown together with the calculated magnon dispersion curves [35,36] and diagrams representing the relevant quasiparticle scattering processes in the system. (a) The process of parametric pumping is shown by orange arrows. The signal of "virtual pump" magnons is visible at the pumping frequency $\omega_{\rm pump}$. The parametrically excited real magnons, marked by magenta dots, are outside the observation region. "Virtual double-bottom" magnons at the frequency $2\omega_{\rm bot}$ arise due to the confluence of "bottom" magnons at $\omega_{\rm bot}$. The three types of confluence processes are indicated by pairs of green arrows. (b) Processes of four-wave interaction of bottom magnons with phase-correlated pairs of parametric magnons leading to the appearance of "virtual top" magnons at the frequency $\omega_{\rm top}$ are pairwise shown by the solid and dotted blue arrows [37].

of our BLS setup at $\approx 2 \times 10^5$ cm^{-1}. Nevertheless, these magnons are definitely present in the system [31], being responsible for the appearance of magnons at the bottom of the frequency spectrum [25,44], which are clearly visible as extremely intense BLS signals.

In our previous studies [45–48], the magnon gas thermalization and BEC formation were developing in close interactions with the phonon bath [46,49,50], and leading to accumulation of hybrid magnon-phonon quasiparticles. In the present experiments, we observe no such phenomenon because the width of the pumping area is small, and the strong efflux of these quasiparticles leads to large losses for them [45].

Two more spots at $\omega_{\rm top} = \omega_{\rm pump} - \omega_{\rm bot}$ and $q_{\rm top} = \pm q_{\rm bot}$, have a more sophisticated origin, which we discuss below within the classical Hamiltonian

formalism convenient for description of nonlinear processes at large occupation numbers.

The classical Hamiltonian formalism is based on the equation of motion for the complex canonical wave amplitudes a_q and a_q^*, which are classical limits of the Bose creation and annihilation operators $\hat{a}_q$ and $\hat{a}_q^\dagger$ [26,27,29]:

$$\frac{da_q(t)}{dt} = -i\frac{\delta\mathcal{H}}{\delta a_q^*(t)}, \tag{1}$$

where $\mathcal{H}$ is the Hamiltonian function, called for brevity the Hamiltonian. As shown, for example, in Refs. [36,51] the classical Landau-Lifshitz equation [52] governing the motion of the magnetic momentum $\boldsymbol{M}(\boldsymbol{r}, t)$ can be represented in the Hamiltonian form (1) using the classical analog of the Holstein-Primakoff transformation from the spin operators to the Bose operators.

For weakly interacting waves, $\mathcal{H}$ can be expanded in a_q and a_q^* as $\mathcal{H} = \mathcal{H}_2 + \mathcal{H}_{\text{int}}$. The quadratic Hamiltonian $\mathcal{H}_2 = \sum_q \omega_q a_q a_q^*$ describes the free propagation of noninteracting waves with the dispersion law ω_q: $a_q(t) \propto \exp[-i\omega_q t]$. The interaction Hamiltonian $\mathcal{H}_{\text{int}} = \mathcal{H}_3 + \mathcal{H}_4$, includes

$$\mathcal{H}_3 = \frac{1}{2}\sum_{1,2,3}\left[V^{3}_{1,2}a_1a_2a_3^* + (V^{3}_{1,2})^* a_1^*a_2^*a_3\right]\Delta^{3}_{1,2}, \tag{2a}$$

$$\mathcal{H}_4 = \frac{1}{4}\sum_{1,2,3,4} T^{3,4}_{1,2}a_1a_2a_3^*a_4^*\Delta^{3,4}_{1,2}. \tag{2b}$$

Here, $V^{3}_{1,2}$ and $T^{3,4}_{1,2}$ are three- and four-wave interaction amplitudes. The Kronecker symbols $\Delta^{3}_{1,2}$ and $\Delta^{3,4}_{1,2}$ are equal to 1 if the sum of "superscript" wave vectors equals the sum of "subscript" wave vectors, and zero otherwise, taking care of wave vector conservation. For shortness, here we use the notation $\boldsymbol{j} \equiv \boldsymbol{q}_j$, with $j = 1, 2, 3, 4$.

The close analogy between the classical Hamiltonian and a quantum mechanical description allows for a physically transparent interpretation of the interactions $\mathcal{H}_3$ and $\mathcal{H}_4$. Namely, $\mathcal{H}_3$ describes the process of the confluence of two waves (or two quasiparticles, such as magnons, phonons, etc.) with the wave vectors $\boldsymbol{q}_1$ and $\boldsymbol{q}_2$ into one wave with the wave vector $\boldsymbol{q}_3 = \boldsymbol{q}_1 + \boldsymbol{q}_2$, two magnons $\Rightarrow$ one magnon [see Fig. 2(a)], and the inverse process of decay of the $\boldsymbol{q}_3$ wave into a pair of $\boldsymbol{q}_1$ waves and $\boldsymbol{q}_2$ waves, one magnon $\Rightarrow$ two magnons [see Fig. 2(b)]:

$$\omega_1 + \omega_2 \Leftrightarrow \omega_3. \tag{3}$$

Hamiltonian $\mathcal{H}_4$ is responsible for the four-magnon scattering (two magnons $\Leftrightarrow$ two magnons) [see Fig. 2(c)] with the conservation laws

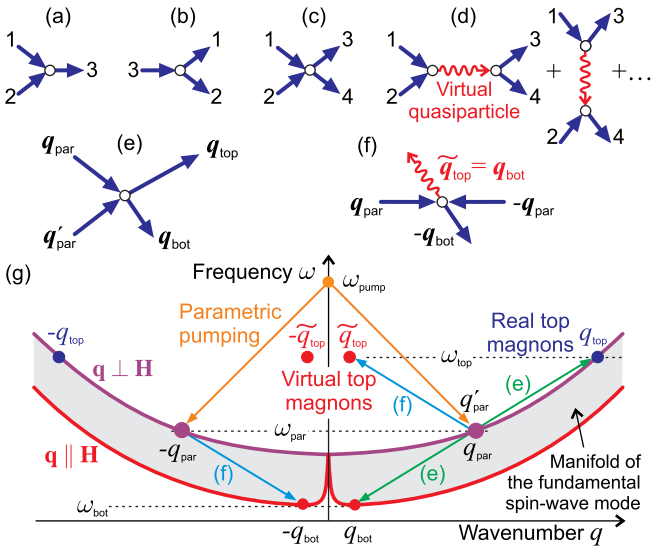

FIG. 2. Graphical representation of multiwave scattering processes. Three-wave confluence (a) and splitting (b) processes given by Eq. (3). (c) The four-wave scattering process given by Eq. (4). (d) The first (see Ref. [53]) and second contribution to the four-magnon scattering process in the second-order perturbation approach in the three-wave Hamiltonian, Eq. (2a). The red wavy lines show virtual quasiparticles, mediating these processes. All six contributions can be found, for example, in Eq. (1.1.32) from Ref. [27]. (e) Diagram of the four-magnon scattering [Eq. (7)] leading to the kinetic instability of real magnons. (f) Diagram of the four-magnon scattering [Eq. (7)] that leads to the excitation of the virtual top magnons. (g) The scattering processes shown in panels (e) and (f) are schematically represented in the magnon spectrum by pairs of green and blue arrows [54].

$$\omega_1 + \omega_2 \Leftrightarrow \omega_3 + \omega_4, \qquad q_1 + q_2 = q_3 + q_4. \tag{4}$$

As a general rule, the three-magnon processes (two $\Leftrightarrow$ one) are more efficient [26]. When they are forbidden by the conservation law (3), one has to account for weaker scattering processes (two $\Leftrightarrow$ two) [Eq. (4)]. Nevertheless, three-wave processes cannot be ignored in this case either. To see this, we examine Eq. (1) with the Hamiltonian (2) away from resonances. The latter allows us not to take into account the wave damping:

$$\left[\frac{d}{dt} + i\omega_q\right]a_q = -\frac{i}{2}\sum_{1,2} V^{q}_{1,2}\Delta^{q}_{1,2}a_1a_2 - i\sum_{2,3}(V^{3}_{q,2})^*\Delta^{3}_{q,2}a_2^*a_3 - \frac{i}{2}\sum_{1,2,3} T^{3,q}_{1,2}a_1a_2a_3^*\Delta^{3,q}_{1,2}. \tag{5}$$

The first term in the right-hand side of Eq. (5) is the sum $\sum_{1,2}$ of off-resonant forces F_{12}, each having the wave vector $\boldsymbol{q}_1 + \boldsymbol{q}_2$ and the frequency $\omega_1 + \omega_2$. Each partial

force F_{12} stirs up a wave with wave vector $\boldsymbol{q}_1 + \boldsymbol{q}_2$, the eigenfrequency $\omega_{12} \equiv \omega(\boldsymbol{q}_1 + \boldsymbol{q}_2)$, and amplitude a_{12}. Far away from resonance, $a_{12} \propto F_{12}/(\omega_{\mathbf{1}} + \omega_{\mathbf{2}} - \omega_{12})$ and, therefore, the total system response is given by the following expression:

$$\sum_{\mathbf{1},2} a_{12} = \sum_{\mathbf{1},2} V_{\mathbf{1},2}^{\mathbf{1}+2} a_{\mathbf{1}} a_{\mathbf{2}} [2(\omega_{\mathbf{1}} + \omega_{\mathbf{2}} - \omega_{12})]^{-1}. \quad (6)$$

Taking $a_{\mathbf{1}}$ and $a_{\mathbf{2}}$ as $a_{\pm q_\parallel}$, we find the amplitudes of the virtual double magnons discussed above. One can say that the interaction process of $\boldsymbol{q}_1$ quasiparticles and $\boldsymbol{q}_2$ quasiparticles nonresonantly excites a wave perturbation of a nonlinear medium—virtual quasiparticles with a total amplitude given by Eq. (6). Note that these virtual quasiparticles can decay into two real quasiparticles $\boldsymbol{q}_3$ and $\boldsymbol{q}_4$ with frequencies $\omega_{\mathbf{3}}$ and $\omega_{\mathbf{4}}$, resulting in the effective four-wave scattering process [53] schematically shown in Fig. 2(d).

Returning to the analysis of our experimental results, note that in our geometry and for $H = 1350$ Oe the high population of the bottom magnons is the result of the so-called kinetic instability [25,38,55]: a four-magnon process (4) of decay of parametric magnons with frequency $\omega_{\mathbf{1}} = \omega_{\mathbf{2}} = \omega_{\text{par}} = \omega_{\text{pump}}/2$ and wave vectors $\boldsymbol{q}_1 = \boldsymbol{q}_{\text{par}}$, and $\boldsymbol{q}_2 = \boldsymbol{q}'_{\text{par}}$ into a pair of the bottom and the so-called "top" magnons with frequencies ω_{bot} and ω_{top} [see Fig. 2(e)]. Note that $\boldsymbol{q}_{\text{par}}$ does not necessarily belong to the same pair of parametrically generated magnons for which $\boldsymbol{q}_{\text{par}} + \boldsymbol{q}'_{\text{par}} = 0$. If so, one expects

$$\omega_{\mathbf{1}} + \omega_{\mathbf{2}} = \omega_{\text{bot}} + \omega_{\text{top}} = \omega_{\text{pump}}, \quad \text{and} \quad (7a)$$

$$\boldsymbol{q}_1 + \boldsymbol{q}_2 = \boldsymbol{q}_{\text{bot}} + \boldsymbol{q}_{\text{top}}. \quad (7b)$$

Assuming a rough estimate that $\omega_{\text{top}} \gg \omega_{\text{bot}}$, we conclude that, as shown in Fig. 2(g) with two blue circles, $q_{\text{top}} > q_{\text{par}}$. It means that the top magnons lie outside the sensitivity region of our BLS setup, i.e., they are invisible in Fig. 1. This raises the crucial question: What is the origin of the two spots in Fig. 1(b) at the "correct" frequency $\omega_{\text{top}} = \omega_{\text{pump}} - \omega_{\text{bot}}$, which is consistent with Eq. (7a), but with the experimentally observed wave vectors $\tilde{\boldsymbol{q}}_{\text{top}} = \pm\boldsymbol{q}_{\text{bot}}$, which completely disagree with Eq. (7b)?

To resolve this controversy, we note that the theory of kinetic instability is formulated in the framework of the weak-wave kinetic equation, which assumes weak correlations of the wave phases. As a result, the scattering (4) of real magnons has a stochastic nature and appears only as a second-order perturbation of the four-wave interaction amplitudes $T_{\mathbf{1},2}^{\mathbf{3},4}$ [Eq. (2b)]. Nevertheless, in our particular case with a large population of parametric magnons, the scattering waves have strong externally determined phase correlations. As shown in the S-theory [27], the energy flux from an external spatial homogeneous pumping field to parametric magnons is proportional to $\langle a_{\boldsymbol{q}_{\text{par}}} a_{-\boldsymbol{q}_{\text{par}}} \exp(i\omega_{\text{pump}} t)\rangle$. As a result, in the competition of parametric pairs, only the pairs with the maximum energy flux from the pump field survive, i.e., pairs with the full phase correlation, for which $|\langle a_{\boldsymbol{q}_{\text{par}}} a_{-\boldsymbol{q}_{\text{par}}} \exp(i\omega_{\text{pump}} t)\rangle| = \langle |a_{\boldsymbol{q}_{\text{par}}}|^2\rangle \equiv n_{\boldsymbol{q}_{\text{par}}}$. This allows us to consider a pair of parametric magnons $(a_{\boldsymbol{q}_{\text{par}}} a_{-\boldsymbol{q}_{\text{par}}})$ as a "single" wave object with the frequency $2\omega_{\text{par}} = \omega_{\text{pump}}$ and phase being the sum of the phases of the waves composing the pair. Therefore, owing to its dynamic nature, the four-wave scattering process (4) with $\boldsymbol{q}_1 = -\boldsymbol{q}_2$, $\boldsymbol{q}_3 = \mp\boldsymbol{q}_{\text{bot}}$, and $\boldsymbol{q}_4 = \tilde{\boldsymbol{q}}_{\text{top}} = \pm\boldsymbol{q}_{\text{bot}}$ is much stronger than stochastic scattering (4) with $\boldsymbol{q}_1 \neq -\boldsymbol{q}_2$, being now proportional to the first power of the interaction amplitude $T_{\mathbf{1},2}^{\mathbf{3},4}$. One can see this from the last term in the right-hand side of Eq. (5), which describes a driving force

$$F_{\text{virt}}(\omega, \pm\boldsymbol{q}_{\text{bot}}) = \sum_{\boldsymbol{q}_{\text{par}}} T_{\boldsymbol{q}_{\text{par}}, -\boldsymbol{q}_{\text{par}}}^{\mp\boldsymbol{q}_{\text{bot}}, \pm\boldsymbol{q}_{\text{bot}}} a_{\boldsymbol{q}_{\text{bot}}}^* a_{\boldsymbol{q}_{\text{par}}} a_{-\boldsymbol{q}_{\text{par}}} \quad (8)$$

having the same frequency $\omega_{\text{top}} = \omega_{\text{pump}} - \omega_{\text{bot}}$ as that of real top magnons [see Eq. (7a)] and wave vector $\tilde{\boldsymbol{q}}_{\text{top}} = \pm\boldsymbol{q}_{\text{bot}}$.

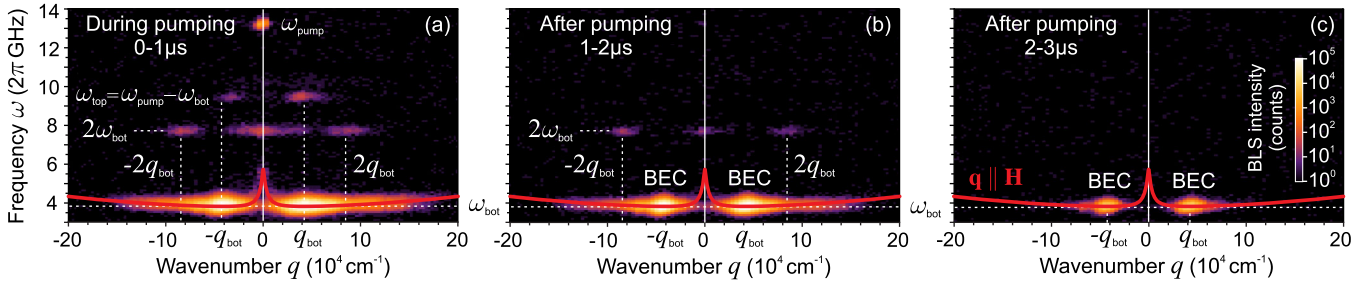

FIG. 3. Time evolution of the BLS spectra of the real and virtual magnons. (a) During the pumping microwave pulse, the virtual top magnons at $\omega_{\text{top}} = \omega_{\text{pump}} - \omega_{\text{bot}}$ are visible alongside with double-bottom virtual magnons at $2\omega_{\text{bot}}$. (b) Soon after the pumping pulse, the virtual top magnons disappear, and only double-bottom virtual magnons are visible as the populations of magnon BECs at ω_{bot} are still large. (c) 2 μs after the pumping pulse, only magnon BECs are visible. Owing to the small magnon quantity, virtual magnons are not observable. All panels: the red solid curves show the calculated dispersion curves of magnons with uniform distributions of dynamic magnetization over the thickness of the YIG film and propagating in the film plane along the magnetization field $\boldsymbol{H}$.

This force should off-resonantly excite "virtual top" magnons [see Figs. 2(f) and 2(g)] with amplitude

$$\tilde{a}_{\mathrm{top}}(\omega_{\mathrm{top}}, \pm\boldsymbol{q}_{\mathrm{bot}}) = F_{\mathrm{virt}}(\omega, \pm\boldsymbol{q}_{\mathrm{bot}})/[2(\omega_{\mathrm{bot}} - \omega_{\mathrm{par}})]. \quad (9)$$

They are visible in Fig. 1 at $\omega = \omega_{\mathrm{top}}$ [56].

It is worth noting that such an enhancement of the efficiency of nonlinear processes in the case of phase-correlated waves is not a specific feature of the magnon system. For example, it is known in quantum optics for simpler cases when only a few waves are involved in the interaction process [57].

To further confirm the origin of different groups of virtual magnons, we studied their evolution after the pumping is turned off. Figure 3 presents the BLS spectra of the real and virtual magnons at different moments of time. Figure 3(a) shows spectra during the pumping process (same as presented in Fig. 1, for reference). Figure 3(b) refers to the time interval $t = (1 - 2)$ μs after the pumping power has been turned off and the rapidly relaxing parametric magnons have disappeared. Therefore, we do not see the pump and top virtual magnons, forced either directly by the pumping magnetic field or through the parametric magnons, as seen in Fig. 2(f). The signal of the top virtual magnons disappears in a time not exceeding 20 ns. This value correlates well with earlier measurements of the scattering time of a group of parametrically pumped magnons, which in the BEC experiments was close to 10 ns [23]. Nevertheless, the double-bottom virtual magnons are still there, forced only by the bottom real magnons. They disappear only later [see Fig. 3(c)], when the number of the (real) bottom magnons becomes too small to force the double magnons above a measurable level. Thus, the time evolution of the virtual magnons confirms the mechanism of their excitation suggested in our Letter.

Traditionally, nonlinear-wave interactions are investigated via observation of real quasiparticles—quanta of freely propagating waves, i.e., eigenmodes of the nonlinear medium. In our experiments with highly populated magnon gases in a ferromagnetic YIG film, we found several types of virtual magnons—quanta of off-resonant spin waves—driven by real magnons through the appropriate nonlinearity. We show that virtual quasiparticles (virtual magnons in our case) may be the end result of a new type of nonlinear processes in systems with narrow intense packets of quasiparticles. In particular, we discovered a four-wave interaction involving pairs of parametric waves with opposite wave vectors and a magnon Bose-Einstein condensate. This process is strongly enhanced by phase correlation in parametric pairs and BECs. The considered interactions that lead to the appearance of virtual quasiparticles contribute to the behavior of nonlinear systems, and are useful for the identification of physical processes in them. Furthermore, the study of various types of virtual and real quasiparticles and their correlation-enhanced interactions is necessary both in the classical [58,59] and quantum [58,60–62] limits, for example, for their application in new information transfer and data processing technologies, including quantum magnonics [58,60–62] and coherent quantum optics (see, e.g., Ref. [57] and references therein).

This study was funded by the Deutsche Forschungsgemeinschaft (DFG, German Research Foundation)—TRR 173/2–268565370 Spin + X (Project B04). D. A. B. acknowledges support from Grant No. ECCS-2138236 from the National Science Foundation of the United States. V. S. L. was in part supported by NSF-BSF Grant No. 2020765. We thank R. Verba, P. Pirro, P. Sukhachov and M. Fleischhauer for fruitful discussions.

*victor.lvov@gmail.com
†anna.pomyalov@weizmann.ac.il
‡dbozhko@uccs.edu
§hilleb@rptu.de
‖serha@rptu.de

[1] S. Bartusek, K. Kornhuber, and M. Ting, 2021 North American heatwave amplified by climate change-driven nonlinear interactions, Nat. Clim. Change **12**, 1143 (2022).
[2] C. Federrath, The turbulent formation of stars, Phys. Today **71**, No. 6, 38 (2018).
[3] M. Martinelli *et al.*, Euclid: Impact of non-linear and baryonic feedback prescriptions on cosmological parameter estimation from weak lensing cosmic shear, Astron. Astrophys. **649**, A100 (2021).
[4] C. Koerner, R. Dreyer, M. Wagener, N. Liebing, H. G. Bauer, and G. Woltersdorf, Frequency multiplication by collective nanoscale spin-wave dynamics, Science **375**, 1165 (2022).
[5] D. Turenne *et al.*, Nonequilibrium sub–10 nm spin-wave soliton formation in FePt nanoparticles, Sci. Adv. **8**, eabn0523 (2022).
[6] J. C. Gartside, K. D. Stenning, A. Vanstone, H. H. Holder, D. M. Arroo, T. Dion, F. Caravelli, H. Kurebayashi, and W. R. Branford, Reconfigurable training and reservoir computing in an artificial spin-vortex ice via spin-wave fingerprinting, Nat. Nanotechnol. **17**, 460 (2022).
[7] J. Q. Anderson, P. A. P. Janantha, D. A. Alcala, M. Wu, and L. D. Carr, Physical realization of complex dynamical pattern formation in magnetic active feedback rings, New J. Phys. **24**, 033018 (2022).
[8] Q. Wang, M. Kewenig, M. Schneider, R. Verba, F. Kohl, B. Heinz, M. Geilen, M. Mohseni, B. Lägel, F. Ciubotaru, C. Adelmann, C. Dubs, S. D. Cotofana, O. V. Dobrovolskiy, T. Brächer, P. Pirro, and A. V. Chumak, A magnonic directional coupler for integrated magnonic half-adders, Nat. Electron. **3**, 765 (2020).
[9] S. Watt and M. Kostylev, Reservoir Computing Using a Spin-Wave Delay-Line Active-Ring Resonator Based on Yttrium-Iron-Garnet Film, Phys. Rev. Appl. **13**, 034057 (2020).

[10] O. V. Prokopenko, D. A. Bozhko, V. S. Tyberkevych, A. V. Chumak, V. I. Vasyuchka, A. A. Serga, O. Dzyapko, R. V. Verba, A. V. Talalaevskij, D. V. Slobodianiuk, Y. V. Kobljanskyj, V. A. Moiseienko, S. V. Sholom, and V. Y. Malyshev, Recent trends in microwave magnetism and superconductivity, Ukr. J. Phys. **64**, 888 (2019).

[11] P. Pirro, V. I. Vasyuchka, A. A. Serga, and B. Hillebrands, Advances in coherent magnonics, Nat. Rev. Mater. **6**, 1114 (2021).

[12] V. Cherepanov, I. Kolokolov, and V. S. L'vov, The saga of YIG: Spectra, thermodynamics, interaction and relaxation of magnons in a complex magnet, Phys. Rep. **229**, 81 (1993).

[13] A. Z. Arsad, A. W. M. Zuhdi, N. B. Ibrahim, and M. A. Hannan, Recent advances in yttrium iron garnet films: Methodologies, characterization, properties, applications, and bibliometric analysis for future research directions, Appl. Sci. **13**, 1218 (2023).

[14] S. O. Demokritov, V. E. Demidov, O. Dzyapko, G. A. Melkov, A. A. Serga, B. Hillebrands, and A. N. Slavin, Bose–Einstein condensation of quasi-equilibrium magnons at room temperature under pumping, Nature (London) **443**, 430 (2006).

[15] O. Dzyapko, P. Nowik-Boltyk, B. Koene, V. E. Demidov, J. Jersch, A. Kirilyuk, T. Rasing, and S. O. Demokritov, High-resolution magneto-optical Kerr-effect spectroscopy of magnon Bose–Einstein condensate, IEEE Magn. Lett. **7**, 1 (2016).

[16] C. Safranski, I. Barsukov, H. K. Lee, T. Schneider, A. A. Jara, A. Smith, H. Chang, K. Lenz, J. Lindner, Y. Tserkovnyak, M. Wu, and I. N. Krivorotov, Spin caloritronic nano-oscillator, Nat. Commun. **8**, 117 (2017).

[17] M. Schneider *et al.*, Bose–Einstein condensation of quasiparticles by rapid cooling, Nat. Nanotechnol. **15**, 457 (2020).

[18] M. Schneider, D. Breitbach, R. O. Serha, Q. Wang, A. A. Serga, A. N. Slavin, V. S. Tiberkevich, B. Heinz, B. Lägel, T. Brächer, C. Dubs, S. Knauer, O. V. Dobrovolskiy, P. Pirro, B. Hillebrands, and A. V. Chumak, Control of the Bose–Einstein Condensation of Magnons by the Spin Hall Effect, Phys. Rev. Lett. **127**, 237203 (2021).

[19] B. Divinskiy, H. Merbouche, V. E. Demidov, K. O. Nikolaev, L. Soumah, D. Gouéré, R. Lebrun, V. Cros, J. B. Youssef, P. Bortolotti, A. Anane, and S. O. Demokritov, Evidence for spin current driven Bose–Einstein condensation of magnons, Nat. Commun. **12**, 6541 (2021).

[20] T. B. Noack, V. I. Vasyuchka, A. Pomyalov, V. S. L'vov, A. A. Serga, and B. Hillebrands, Evolution of room-temperature magnon gas: Toward a coherent Bose–Einstein condensate, Phys. Rev. B **104**, L100410 (2021).

[21] S. M. Rezende, Theory of coherence in Bose–Einstein condensation phenomena in a microwave-driven interacting magnon gas, Phys. Rev. B **79**, 174411 (2009).

[22] A. Seyranian, The swing: Parametric resonance, J. Appl. Math. Mech. **68**, 757 (2004).

[23] A. A. Serga, V. S. Tiberkevich, C. W. Sandweg, V. I. Vasyuchka, D. A. Bozhko, A. V. Chumak, T. Neumann, B. Obry, G. A. Melkov, A. N. Slavin, and B. Hillebrands, Bose–Einstein condensation in an ultra-hot gas of pumped magnons, Nat. Commun. **5**, 3452 (2014).

[24] P. Clausen, D. A. Bozhko, V. I. Vasyuchka, B. Hillebrands, G. A. Melkov, and A. A. Serga, Stimulated thermalization of a parametrically driven magnon gas as a prerequisite for Bose–Einstein magnon condensation, Phys. Rev. B **91**, 220402(R) (2015).

[25] A. J. E. Kreil, D. A. Bozhko, H. Y. Musiienko-Shmarova, V. I. Vasyuchka, V. S. L'vov, A. Pomyalov, B. Hillebrands, and A. A. Serga, From Kinetic Instability to Bose–Einstein Condensation and Magnon Supercurrents, Phys. Rev. Lett. **121**, 077203 (2018).

[26] V. E. Zakharov, V. S. L'vov, and G. Falkovich, *Kolmogorov Spectra of Turbulence I. Wave Turbulence*, Springer Series in Nonlinear Dynamics (Springer-Verlag, Berlin, 1992), 10.1007/978-3-642-50052-7.

[27] V. S. L'vov, *Wave Turbulence Under Parametric Excitation. Applications to Magnets*, Springer Series in Nonlinear Dynamics (Springer-Verlag, Berlin, 1994), 10.1007/978-3-642-75295-7.

[28] K. L. Livesey, M. P. Kostylev, and R. L. Stamps, Parametric spin wave excitation and cascaded processes during switching in thin films, Phys. Rev. B **75**, 174427 (2007).

[29] S. Nazarenko, *Wave Turbulence*, Lecture Notes in Physics Vol. 825 (Springer-Verlag, Berlin, 2011), 10.1007/978-3-642-15942-8.

[30] B. Hillebrands, Brillouin light scattering from layered magnetic structures, in *Light Scattering in Solids VII: Crystal-Field and Magnetic Excitations*, edited by M. Cardona and G. Güntherodt (Springer, New York, 2000), pp. 174–289, 10.1007/BFb0103386.

[31] A. A. Serga, C. W. Sandweg, V. I. Vasyuchka, M. B. Jungfleisch, B. Hillebrands, A. Kreisel, P. Kopietz, and M. P. Kostylev, Brillouin light scattering spectroscopy of parametrically excited dipole-exchange magnons, Phys. Rev. B **86**, 134403 (2012).

[32] R. Mock, B. Hillebrands, and R. Sandercock, Construction and performance of a Brillouin scattering set-up using a triple-pass tandem Fabry–Perot interferometer, J. Phys. E **20**, 656 (1987).

[33] D. A. Bozhko, H. Y. Musiienko-Shmarova, V. S. Tiberkevich, A. N. Slavin, I. I. Syvorotka, B. Hillebrands, and A. A. Serga, Unconventional spin currents in magnetic films, Phys. Rev. Res. **2**, 023324 (2020).

[34] C. W. Sandweg, M. B. Jungfleisch, V. I. Vasyuchka, A. A. Serga, P. Clausen, H. Schultheiss, B. Hillebrands, A. Kreisel, and P. Kopietz, Wide-range wavevector selectivity of magnon gases in Brillouin light scattering spectroscopy, Rev. Sci. Instrum. **81**, 073902 (2010).

[35] B. A. Kalinikos and A. N. Slavin, Theory of dipole-exchange spin wave spectrum for ferromagnetic films with mixed exchange boundary conditions, J. Phys. C **19**, 7013 (1986).

[36] S. M. Rezende, *Fundamentals of Magnonics*, Lecture Notes in Physics Vol. 969 (Springer, Cham, 2020), 10.1007/978-3-030-41317-0.

[37] Additional process leading to the appearance of "virtual top" magnons is the scattering process in which the parametric magnon q_{par} scatters to the virtual state $(\omega_{\mathrm{top}}, -q_{\mathrm{bot}})$, and the magnon $-q_{\mathrm{par}}$ to the state $(\omega_{\mathrm{bot}}, q_{\mathrm{bot}})$, and also symmetric to it, when the parametric magnon q_{par} scatters to the state $(\omega_{\mathrm{bot}}, -q_{\mathrm{bot}})$, and the magnon $-q_{\mathrm{par}}$ to the virtual state $(\omega_{\mathrm{top}}, q_{\mathrm{bot}})$.

[38] A. V. Lavrinenko, V. S. L'vov, G. A. Melkov, and V. B. Cherepanov, "Kinetic" instability of a strongly nonequilibrium system of spin waves and tunable radiation of a

ferrite, Sov. Phys. JETP **54**, 542 (1981), http://jetp.ras.ru/cgi-bin/e/index/e/54/3/p542?a=list.

[39] O. Dzyapko, V. E. Demidov, S. O. Demokritov, G. A. Melkov, and V. L. Safonov, Monochromatic microwave radiation from the system of strongly excited magnons, Appl. Phys. Lett. **92**, 162510 (2008).

[40] In fact, in these spectral regions, there are thickness spin-wave modes [11,35]. Even at close to zero values of their wave numbers $q_{\|}$ in the film plane, such modes with large indices can have high frequencies due to the contribution of the exchange interaction caused by the large wave number $q_{\perp}$ in the direction of the normal to the film plane. However, as shown in Ref. [33], these modes do not contribute to the BLS spectrum in our experimental conditions precisely because of the large $q_{\perp}$. In addition, all scattering processes considered in our Letter are prohibited for these modes due to the inability to satisfy the momentum conservation law. The confluence of two magnons with $q_{\perp} = 0$ (BEC magnons) cannot give rise to a magnon with $q_{\perp} \neq 0$. Such a magnon also cannot be produced in the process of four-magnon scattering, in which for the other three magnons (two parametric and one BEC magnon) $q_{\perp} = 0$.

[41] M. Geilen, R. Verba, A. Nicoloiu, D. Narducci, A. Dinescu, M. Ender, M. Mohseni, F. Ciubotaru, M. Weiler, A. Müller, B. Hillebrands, C. Adelmann, and P. Pirro, Parametric excitation and instabilities of spin waves driven by surface acoustic waves, arXiv:2201.04033.

[42] M. Sushruth, M. Grassi, K. Ait-Oukaci, D. Stoeffler, Y. Henry, D. Lacour, M. Hehn, U. Bhaskar, M. Bailleul, T. Devolder, and J.-P. Adam, Electrical spectroscopy of forward volume spin waves in perpendicularly magnetized materials, Phys. Rev. Res. **2**, 043203 (2020).

[43] T. Sebastian, T. Brächer, P. Pirro, A. A. Serga, B. Hillebrands, T. Kubota, H. Naganuma, M. Oogane, and Y. Ando, Nonlinear Emission of Spin-Wave Caustics from an Edge Mode of a Microstructured $Co_2Mn_{0.6}Fe_{0.4}Si$ Waveguide, Phys. Rev. Lett. **110**, 067201 (2013).

[44] D. A. Bozhko, P. Clausen, A. V. Chumak, Y. V. Kobljanskyj, B. Hillebrands, and A. A. Serga, Formation of Bose–Einstein magnon condensate via dipolar and exchange thermalization channels, Low Temp. Phys. **41**, 801 (2015).

[45] D. A. Bozhko, P. Clausen, G. A. Melkov, V. S. L'vov, A. Pomyalov, V. I. Vasyuchka, A. V. Chumak, B. Hillebrands, and A. A. Serga, Bottleneck Accumulation of Hybrid Magnetoelastic Bosons, Phys. Rev. Lett. **118**, 237201 (2017).

[46] D. A. Bozhko, V. I. Vasyuchka, A. V. Chumak, and A. A. Serga, Magnon-phonon interactions in magnon spintronics (Review article), Low Temp. Phys. **46**, 383 (2020).

[47] P. Frey, D. A. Bozhko, V. S. L'vov, B. Hillebrands, and A. A. Serga, Double accumulation and anisotropic transport of magnetoelastic bosons in yttrium iron garnet films, Phys. Rev. B **104**, 014420 (2021).

[48] V. Hahn, P. Frey, A. A. Serga, V. I. Vasyuchka, B. Hillebrands, P. Kopietz, and A. Rückriegel, Accumulation of magnetoelastic bosons in yttrium iron garnet: Kinetic theory and wave-vector-resolved Brillouin light scattering, Phys. Rev. B **105**, 144421 (2022).

[49] J. Hick, F. Sauli, A. Kreisel, and P. Kopietz, Bose–Einstein condensation at finite momentum and magnon condensation in thin film ferromagnets, Eur. Phys. J. B **78**, 429 (2010).

[50] A. Rückriegel, P. Kopietz, D. A. Bozhko, A. A. Serga, and B. Hillebrands, Magnetoelastic modes and lifetime of magnons in thin yttrium iron garnet films, Phys. Rev. B **89**, 184413 (2014).

[51] V. Zakharov, V. S. L'vov, and S. Starobinets, Spin-wave turbulence beyond the parametric excitation threshold, Sov. Phys. Usp. **17**, 896 (1975).

[52] L. D. Landau and E. M. Lifshitz, On the theory of the dispersion of magnetic permeability in ferromagnetic bodies, Phys. Z. Sowjetunion **8**, 153 (1935).

[53] By substituting $a(\boldsymbol{q}_1 + \boldsymbol{q}_2)$ from Eq. (6) into Eq. (2a) for the Hamiltonian $\mathcal{H}_3$ one can find an additional contribution to the four-wave interaction amplitude $\delta T_{\mathbf{1,2}}^{\mathbf{3,4}} = V_{\mathbf{1,2}}^{\mathbf{1+2}} V_{\mathbf{1+2}}^{\mathbf{3,4}\,*} (\omega_{\mathbf{1}} + \omega_{\mathbf{2}} - \omega_{\mathbf{1+2}})^{-1}$, arising in the second order of the perturbation theory by the amplitude of three-wave processes $V_{\mathbf{1,2}}^{\mathbf{3}}$ through the virtual wave with the frequency $\omega_{\mathbf{V}} = \omega_{\mathbf{1+2}}$: $\omega_{\mathbf{1}} + \omega_{\mathbf{2}} \Rightarrow \omega_{\mathbf{1+2}} \Rightarrow \omega_{\mathbf{3}} + \omega_{\mathbf{4}}$. This process is shown in Fig. 2(d).

[54] At high pumping powers, the parametric magnons and, accordingly, the real top magnons are distributed in the vicinity of their resonant frequencies and along the corresponding isofrequency curves in the wave vector space, as shown in Fig. 2(a) in Ref. [25].

[55] G. A. Melkov and S. V. Sholom, Kinetic instability of spin waves in thin ferrite films, Sov. Phys. JETP **72**, 341 (1991), http://jetp.ras.ru/cgi-bin/e/index/e/72/2/p341?a=list.

[56] It may seem that this BLS signal can also be caused by magnons of thickness spin-wave modes, which could be excited by two-magnon scattering of the real top magnons on static inhomogeneities of the magnetic medium. However, the process of two-magnon scattering does not preserve quasiparticle momenta, which means that such a signal, even if our setup could detect it [40], would be smeared over q space with an intensity distribution determined by the size of the inhomogeneities. Instead, the observed signal is well localized in the vicinity of the magnon BEC wave numbers, as predicted by our model.

[57] P. Türschmann, H. L. Jeannic, S. F. Simonsen, H. R. Haakha, S. Götzinger, V. Sandoghdar, P. Lodahl, and R. Nir, Coherent nonlinear optics of quantum emitters in nanophotonic waveguides, Nanophotonics **10**, 1641 (2019).

[58] M. Silaev, Ultrastrong magnon-photon coupling, squeezed vacuum, and entanglement in superconductor/ferromagnet nanostructures, Phys. Rev. B **107**, L180503 (2023).

[59] J. Bailey, P. Sukhachov, K. Baumgaertl, S. Finizio, S. Wintz, C. Dubs, J. Raabe, D. Grundler, A. Balatsky, and G. Aeppli, Multi-band Bose–Einstein condensate at four-particle scattering resonance, arXiv:2201.11043.

[60] M. Fukami, D. R. Candido, D. D. Awschalom, and M. E. Flatté, Opportunities for long-range magnon-mediated entanglement of spin qubits via on- and off-resonant coupling, PRX Quantum **2**, 040314 (2021).

[61] H. Y. Yuan, S. Zheng, Q. Y. He, J. Xiao, and R. A. Duine, Unconventional magnon excitation by off-resonant microwaves, Phys. Rev. B **103**, 134409 (2021).

[62] B. Heténi, A. Mook, J. Klinovaja, and D. Loss, Long-distance coupling of spin qubits via topological magnons, Phys. Rev. B **106**, 235409 (2022).